J. Electrochem. Sci. Eng. **00(0)** (2023) 000-000; http://dx.doi.org/10.5599/jese.2145

Open Access : : ISSN 1847-9286
www.jESE-online.org

Original scientific paper

Fe_3O_4 nanoparticles decorated reduced graphene oxide&carbon nanotubes-based composite for sensitive detection of imatinib in plasma and urine

Nasim Naderi[1], Bahare Sabeti[1], and Fereshteh Chekin[2,✉]

[1]*Department of Pharmacy, Ayatollah Amoli Branch, Islamic Azad University, Amol, Iran*
[2]*Department of Chemistry, Ayatollah Amoli Branch, Islamic Azad University, Amol, Iran*

Corresponding author: ✉fchekin@yahoo.com; Tel.: ++981 143 217 076

Received: October 25, 2023; Accepted: November 30, 2023; Published: December xx, 2023

Abstract

In this study, a new reduced graphene oxide (rGO) has been synthesized via a facile and environmentally friendly process using Callicarpa maingayi leaf extract. A novel magnetic catalyst based on Fe_3O_4 nanoparticles-reduced graphene oxide&carbon nanotubes ((Fe_3O_4--(rGO&CNT)) was prepared and characterized by hydrothermal method. The Fe_3O_4 nanoparticles with an average size of 25 to 40 nm were placed on carbon nanotubes and reduced graphene oxide sheets, while carbon nanotubes inserted between the reduced graphene oxide sheets effectively prevented their aggregation. The (Fe_3O_4-(rGO&CNT) composite has a large surface area and good electrocatalytic properties, suiting for the detection and determination of imatinib (IM) anticancer drug by voltammetry method. Under optimized conditions, good linearity was achieved in the concentration range of 0.1 to 40 µmol L^{-1} and the limit of detection and sensitivity were 57 nmol L^{-1} and 3.365 µA L µmol^{-1}, respectively. Furthermore, the fabricated sensor demonstrated acceptable reproducible behaviour and accuracy and a high level of stability during all electrochemical tests. In addition, the proposed method was applied for the detection of IM in biological samples and the recoveries were 94.0 to 98.5 %, with relative standard deviations of 2.1 to 4.4 %.

Keywords

Magnetite/carbon nanocomposite, electrochemical sensor; imatinib drug; real samples

Introduction

Cancer is one of the most important diseases facing humanity today. Cancer is lethal because its cells are uncontrolled and proliferate indefinitely and spread throughout the body [1,2]. Cytostatic agents are the most commonly used class of anticancer drugs. Their purpose is to inhibit the growth of cancer cells. However, the widespread use of cytostatic agents has caused some other effects, such as on environmental toxicology [3]. Among them, imatinib (IM), with the chemical structure shown in Figure 1, is a specific inhibitor. Imatinib (4-[(4-methylpiperazin-1-yl) methyl]-N-[4-methyl-

3-[(4-pyridin-3-ylpyrimidin-2-yl)amino]phenyl]benzamide) is used to treat chronic myeloid leukemia (CML) and diseases such as gastrointestinal stromal tumours [4]. Imatinib, known as Gleevec, is a chemotherapy drug used to treat some cancers. This drug was approved by the Food and Drug Administration (FDA) to treat different cancers [5]. By inhibiting the activity of synthetic tyrosine kinase, specifically designed to inhibit Bcr-Abl fusion protein, it reduces cell growth or apoptosis in some cancer cells [6]. IM is a drug for anticancer treatment, used selectively to annihilate cancer cells instead of damaging them by rapidly dividing cells [7].

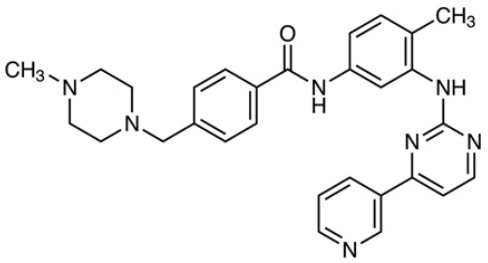

Figure 1. *Chemical structure of imatinib*

A number of analytical techniques have been applied to IM analysis, such as fluorescence, liquid chromatography, capillary electrophoresis and UV-Vis spectroscopy methods [8-12]. Owing to the sites with an electroactive nature on the IM surface, the electrochemical procedure has been offered for this drug detection. Therefore, selecting an appropriate method with sensitivity and efficiency in detection and reducing operating costs to evaluate lower IM values is a challenging endeavour. Several electrochemical investigations based on electrochemical sensors have been performed to date [13-16].

Carbon electrodes have a stable electrochemical window and do not react easily with other substances [17,18]. However, the electrochemical signal of ordinary carbon electrodes is weak, so it is difficult to meet the demand for highly sensitive detection [19]. Modification of the surface of ordinary carbon electrodes is a common method to improve the electrochemical activity of sensors. Recent studies have shown that modification of carbon nanomaterials on the surface of electrodes can increase electrical conductivity. Among carbon nanomaterials, carbon nanotubes (CNTs) are wholly employed as conductors due to their attractive and useful characteristics. The high chemical stability, excellent mechanical properties, high surface area, and prominent electrical conductivity make them appropriate for employment in electrochemical procedures [20]. It is known that CNTs promote electron transfer reactions when used as electrode-modifying material [21]. They display a highly hydrophobic surface by π-conjugative structure. This distinctive feature of CNTs could increase their ability to interact with some compounds *via* hydrophobic and/or π-π bonding.

Reduced graphene oxide (rGO) is a nanostructured material with high surface area, excellent thermal and mechanical stability, and remarkable electrical conductivity [22]. The rGO- has a more specific surface area and can easily be hybridized with Fe_3O_4 nanoparticles to form heterostructures [23]. The Fe_3O_4&rGO nanocomposites, with the advantages of magnetism and conductivity, could be easily adhered to the electrode surface to achieve the direct redox reactions and electrocatalytic behavior of analytes adsorbed on the modified surface [24]. Moreover, the functional groups (COOH and OH) of rGO allow it to conjugate with various molecules and act as an excellent performance carrier, while nanoparticles can be highly dispersed on its surface. The charge transfer at the interface of these hybrid materials can provide a synergistic effect to bring properties different from those of each component [25].

To the best of our knowledge, there are no prior reports in the literature on the electrocatalytic behavior of Fe_3O_4-(rGO&CNT) nanocomposites. In this work, the *Callicarpa maingayi* leaf extract is chosen as a reducing agent to reduce graphene oxide to the reduced graphene oxide (rGO) by a one-step method. By combining CNT tubes, rGO sheets and Fe_3O_4 nanoparticles, an excellent nanocomposite was created with high surface area and good conductivity to improve the surface of electrodes. The prepared modified electrode demonstrated remarkable electrocatalytic activity for the detection of IM in biological samples with reasonable analytical results.

Experimental

Materials

Multi-walled carbon nanotubes (MWCNTs, outer diameter: 20-40 nm, length: 5-15 µm, >97 %) were purchased from Shenzhen Nano-Technologies Port Co., Ltd. (China). Graphene oxide was purchased from Nano Materials Pioneers (Iran). The *Callicarpa maingayi* leaves were obtained from Kuala Lumpur, Malaysia. Imatinib ($C_{29}H_{31}N_7O$, 98 %), potassium hexacyanoferrate (II) ($[K_4Fe(CN)_6$, 98.5 %]), phosphoric acid (H_3PO_4, >99 %), sodium dihydrogen phosphate (NaH_2PO_4, >98 %), disodium hydrogen phosphate (Na_2HPO_4, >99 %), sodium phosphate (Na_3PO_4, >99 %) and graphite powder (99.99 %) were purchased from Sigma-Aldrich (Germany) and used as received. Human plasma samples were kindly provided by the clinical laboratory tests (Amol, Iran). The samples were stored at 4 °C.

Apparatus

Surface morphology and chemical composition of the nanocomposites were examined by a scanning electron microscope of MIRATESCAN-XMU (Czech Republic) combined with EDX (energy-dispersive X-ray spectroscopy) machine. Electrochemical measurements were performed with a potentiostat/galvanostat (Sama 500-c Electrochemical Analysis system, Sama, Iran). A conventional three-electrode configuration consisting of Ag|AgCl|KCl3M as the reference electrode, a platinum wire as the auxiliary electrode and Fe_3O_4-(rGO&CNT) modified CPE as the working electrode was employed. UV-Vis spectra of samples were recorded by UV-Vis spectrophotometer (UV-1900, Shimadzu Co., Japan). X-ray diffraction measurement was recorded on a Bruker D8-Advance X-ray diffractometer (Germany).

Synthesis of Fe_3O_4-(rGO&CNT) composite

The reduced graphene oxide was prepared according to previous works [26,27]. The amount of 10 g of fresh *Callicarpa maingayi* leaves were crushed, transferred into a round bottom flask containing 100 mL ionized water, and then placed in an ultrasound bath (60 kHz frequency) at 50 °C for 60 min. After completion of sonication, the mixture was allowed to cool down to room temperature and filtered to obtain a yellowish-green colour extract. 10 mg GO was added to the 50 mL extract and sonicated for 30 min at 25 °C in order to disperse the GO uniformly throughout the extract. The mixture was refluxed for 6 h at 50 °C until the suspension solution colour changed to brown-black. The product (rGO) was filtrated, washed with water and dried in the oven at 100 °C overnight. To 10 mL of rGO (1 mg mL^{-1}), 10 mg of CNT was added and the mixture was sonicated for 45 min at 25 °C. The product (rGO&CNT) was filtered, washed with water and dried in the oven at 100 °C overnight. For functionalization of rGO&CNT composite by Fe_3O_4 nanoparticles, 5 mg of rGO&CNT was sonicated in 20 mL water at 25 °C for 1 h. Then, 10 mL of iron(II) sulphate heptahydrate ($FeSO_4{\times}7H_2O$) solution (0.1 mol L^{-1}) was added to rGO&CNT suspension solution under

vigorous stirring. The pH of the solution was adjusted to 10 with NaOH, transferred to Teflon-lined stainless steel autoclave, and heated at 180 °C for 8 h. Water was used to wash the sample and then the product (Fe_3O_4-(rGO&CNT)) was dried at 60 °C overnight.

Total phenolic content (TPC)

The total phenolic content absorbed on rGO, rGO&CNT and Fe_3O_4-(rGO&CNT) samples was determined according to the Folin-Ciocalteu spectrophotometric method [28]. The 1 mL of samples (1 mg mL^{-1}) solution was mixed with 2.5 mL of Folin-Ciocalteu reagent 10 vol.% and neutralized with 2 mL of sodium carbonate 7.5 % (W/V). The reaction mixture was incubated at 45 °C for 40 min and the absorbance of solution was measured at 765 nm using a UV-Vis spectrophotometer. The total phenolic content is calculated based on gallic acid. To prepare a calibration curve from gallic acid, the results were expressed in terms of ppm of solutions. The test was done in triplicate.

Fabrication of Fe_3O_4-(rGO&CNT) nanocomposite modified electrode

The carbon paste electrode (CPE) was prepared as described in our previous reports [29,30]. The graphite powder plus paraffin was hand-mixed until a uniformly wetted paste was obtained. Then, the carbon paste was packed into a glass tube (with an internal radius 3 mm). Electrical contact was made by a copper wire. The new electrode surface was obtained by polishing it on a weighing paper. 1 mg of Fe_3O_4-(rGO&CNT) nanocomposite was added to 1 mL of water and sonicated for 30 min. 5 µL of this solution was drop-casted onto the CPE and allowed to dry in an oven at 50 °C for 30 min.

Analysis of plasma and urine

500 µL of human serum plasma or urine was transferred to the electrochemical cell containing 10 mL phosphate buffer solution (PB, 0.1 mol L^{-1}; pH 7.0) and the oxidation current was determined by cyclic voltammetry. Also, the samples were determined by UV-Vis spectroscopy at the wavelength of 243 nm with diluting 500 µL of plasma or urine in 5 mL PB (0.1 mol L^{-1}; pH 7.0).

Results and discussion

Characterization

Figure 2 (A) shows the electrochemical behaviour of *Callicarpa maingayi* leaf extract (100 mg L^{-1}) in 0.1 mol L^{-1} PB, pH 7.0 at CPE. A pair of well-defined redox peaks was obtained in the cyclic voltammogram, where anodic peak potential at ~260 mV and cathodic peak potential at ~220 mV could be ascribed to many phytocompounds redox couples in 0.1 mol L^{-1} PB that oxidize in the potential field. In order to realize the surface functional group information on samples, TPC on rGO, rGO&CNT and Fe_3O_4-(rGO&CNT) was calculated based on gallic acid (GA) with calibration linear function A = 0.022 c_{GA} - 0.008 and R^2 = 0.9915. TPC of rGO, rGO&CNT and Fe_3O_4-(rGO&CNT) was calculated as 0.93, 0.82 and 0.73 ppm, respectively compared with GO (0 ppm). *Callicarpa maingayi* leaf extract is a rich source of phytochemicals such as polyphenols, flavonoids and catechins, and shows remarkable performance as a reducing agent. The phytochemicals present in the *Callicarpa maingayi* leaf extract are of great medicinal value and also environmentally benign.

The formed rGO, rGO&CNT and Fe_3O_4-(rGO&CNT) are characterized by UV-Vis spectroscopy in the range of 200 to 600 nm (Figure 2B). The CNT shows an absorption broad peak at ~270 nm. The absorption peak of the rGO suspension is around 279 nm, which, on interaction with CNT, shifted towards 311 nm for rGO&CNT. The absorption peaks of Fe_3O_4-(rGO&CNT) at 271 nm and 320 nm belong to CNT and rGO, respectively, while the peaks of 361 and 376 nm are in good agreement with

Fe_3O_4 nanoparticles. Thus, the UV-Vis spectrum confirms the presence of the Fe_3O_4-(rGO&CNT) hybrid.

The electrochemical behaviour of CPE electrodes modified with rGO, CNT, rGO&CNT and Fe_3O_4-(rGO&CNT) through drop casting were tested using $[Fe(CN)_6]^{3-/4-}$ redox couple, and presented in Figure 2C. The redox current increased in the presence of Fe_3O_4-(rGO&CNT) and is larger than those recorded for bare CPE and rGO, CNT and rGO&CNT modified CPE. The good electronic properties of rGO and CNT support rapid electron transfer and are most likely responsible for the current enhancement. The real electrochemical active surface area of rGO/CPE, CNT/CPE, rGO&CNT/CPE and Fe_3O_4-(rGO&CNT)/CPE was determined by plotting the oxidation peak current as a function of the square root of the scan rate for $[Fe(CN)_6]^{4-}$ (2 mM). From the slopes of these graphs, the values of active surface area were obtained using equation (1) [27]:

$$A = \text{slope} / (268.6 n^{3/2} D^{1/2} c) \quad (1)$$

where A is the electrochemical active surface area (cm^2), n is the number of electrons transferred (n = 1), D is diffusion coefficient of $[Fe(CN)_6]^{4-}$ (3.09×10^{-6} cm^2 s^{-1}) and c is concentration of $[Fe(CN)_6]^{4-}$. For rGO/CPE, CNT/CPE and rGO&CNT/CPE, active surface area values were 0.19, 0.22 and 0.25 cm^2, respectively, while for Fe_3O_4-(rGO&CNT)/CPE an increased surface area (0.27 cm^2) was obtained. The significantly high electroactive area of Fe_3O_4-(rGO&CNT)/CPE recommends Fe_3O_4-(rGO&CNT) as an efficient substrate to fabricate sensors and biosensors.

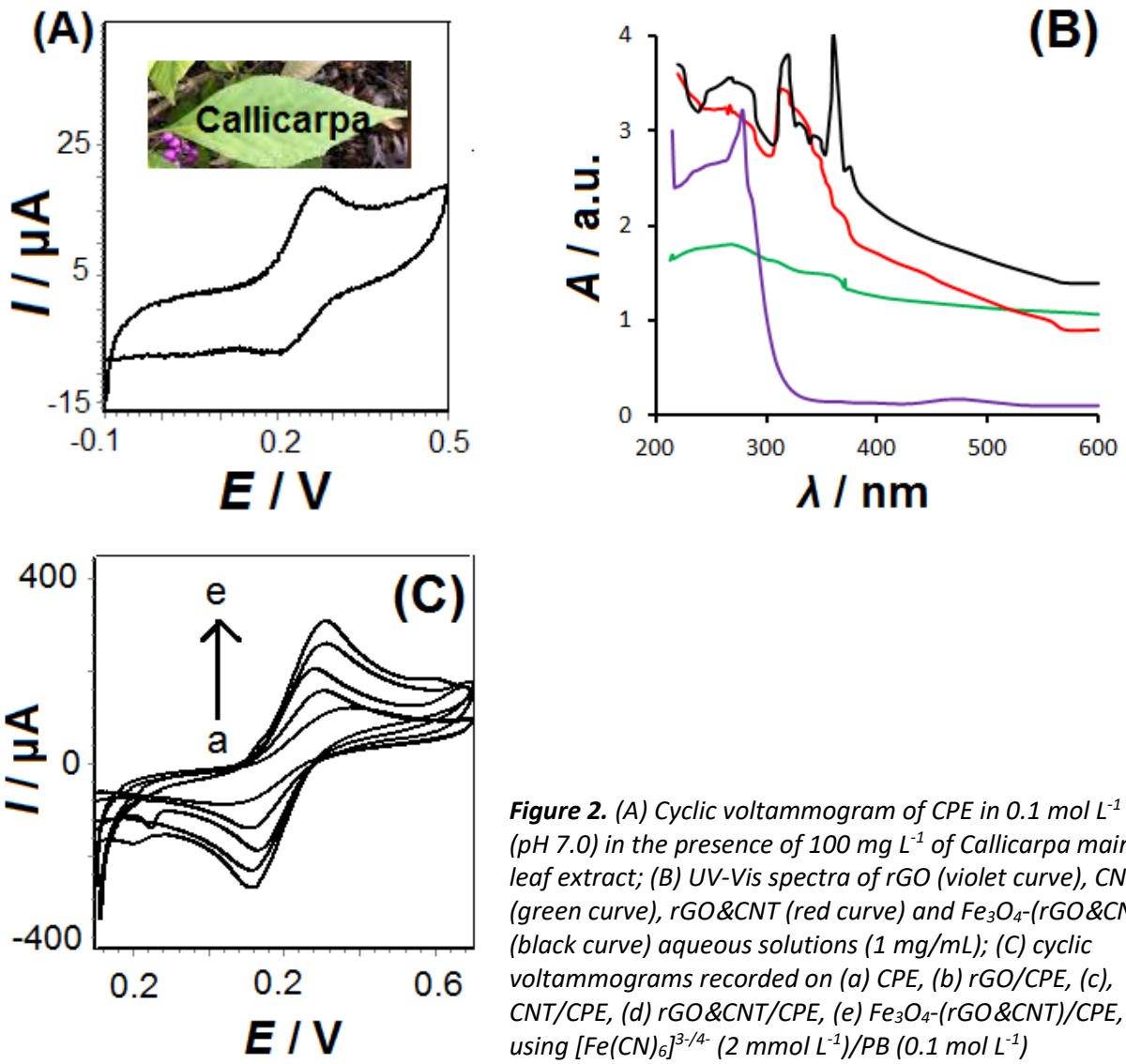

Figure 2. *(A) Cyclic voltammogram of CPE in 0.1 mol L^{-1} PB (pH 7.0) in the presence of 100 mg L^{-1} of Callicarpa maingayi leaf extract; (B) UV-Vis spectra of rGO (violet curve), CNT (green curve), rGO&CNT (red curve) and Fe_3O_4-(rGO&CNT) (black curve) aqueous solutions (1 mg/mL); (C) cyclic voltammograms recorded on (a) CPE, (b) rGO/CPE, (c), CNT/CPE, (d) rGO&CNT/CPE, (e) Fe_3O_4-(rGO&CNT)/CPE, using $[Fe(CN)_6]^{3-/4-}$ (2 mmol L^{-1})/PB (0.1 mol L^{-1})*

The powder X-ray diffraction (XRD) could provide effective evidence of synthesized Fe_3O_4--(rGO&CNT) hybrid. Figure 3 shows the XRD patterns of rGO, CNT, rGO&CNT and Fe_3O_4-(rGO&CNT) samples. As seen, rGO shows a diffraction peak at ~26° corresponding to the (002) reflection. CNT exhibited an intense diffraction pattern at 25.6° and a weak pattern at 44.4° originating from the (002) and (100), respectively, which, on interaction with rGO, shifted towards 2θ values of 26.14 and 43.3° for rGO&CNT. The diffraction peaks at 30.5, 36.1, 43.4, 53.8, 57.5 and 63.1 of Fe_3O_4-(rGO&CNT) could be indexed as that of face-centered cubic (fcc) spinel phase of Fe_3O_4 nanoparticles (JCPDS:19-0629) [31].

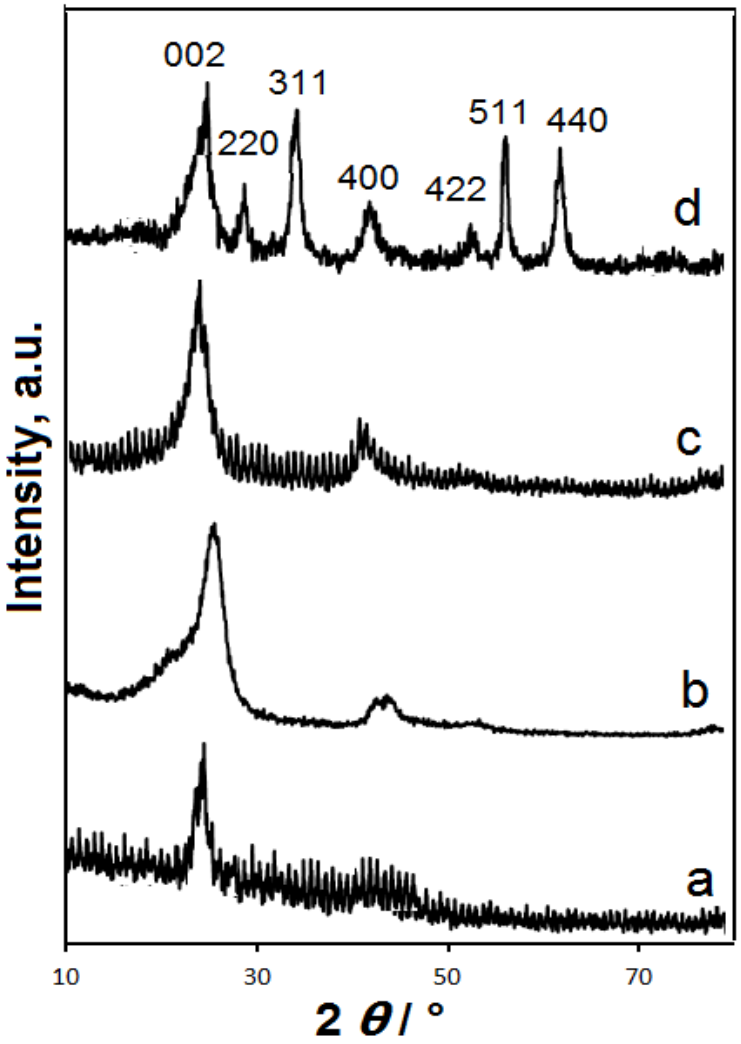

Figure 3. *XRD patterns of (a) rGO, (b) CNT, (c) rGO&CNT and (d) Fe_3O_4-(rGO&CNT)*

The morphology of rGO, CNT, rGO&CNT and Fe_3O_4-(rGO&CNT) is characterized with FE-SEM. As seen in Figure 4, the rGO shows the multilayered sheets onto each other, a rougher surface and wave-shaped corrugated structures. The CNTs are tubular and have open macropore structures. In contrast, the surface of rGO&CNT appears coarse, indicating most of the CNTs were relatively well dispersed in the rGO matrix. The image of Fe_3O_4-(rGO&CNT) shows that the rGO&CNT composite is decorated by sphere shape Fe_3O_4 nanoparticles with a diameter in the range of 25 to 40 nm.

Figure 5 illustrates the elemental analysis (EDX) of synthesized Fe_3O_4-(rGO&CNT) nanocomposite. The specific peak of Fe element in Figure 5 (a) indicates the presence of Fe_3O_4 nanoparticles on the rGO&CNT nanostructure. Also, the homogenous distribution of Fe can be seen in the elemental mapping of Fe_3O_4-(rGO&CNT) presented in Figure 5 (b).

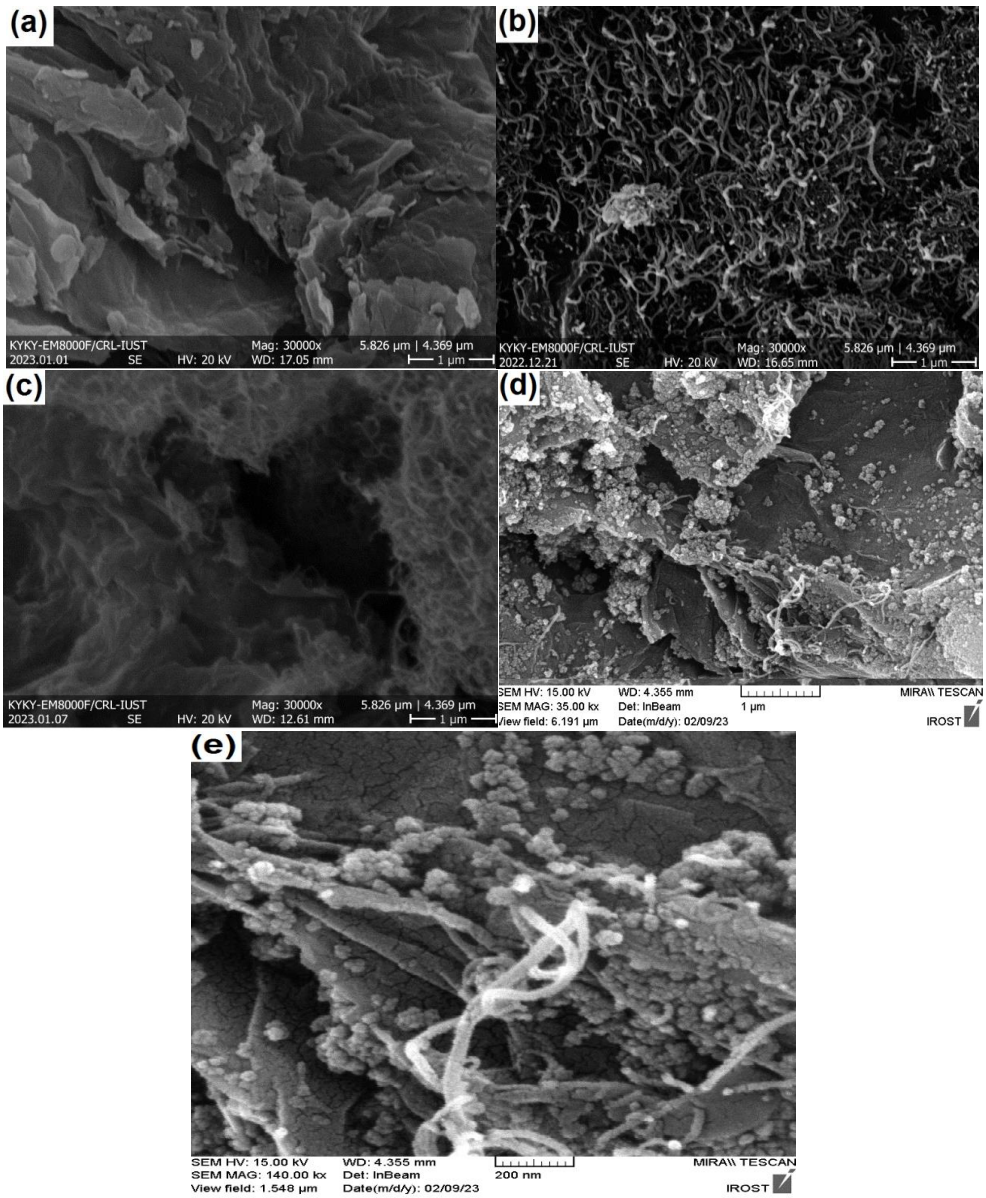

Figure 4. *FE-SEM images of: (a) rGO; (b) CNT; (c) rGO&CNT; (d) Fe_3O_4-(rGO&CNT); (e) Fe_3O_4-(rGO&CNT) with larger magnification*

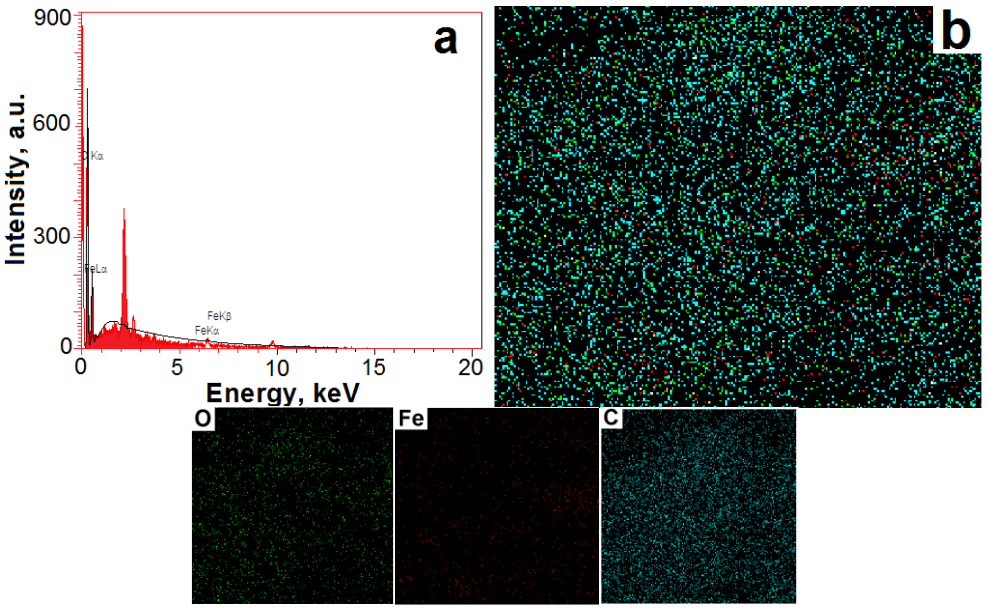

Figure 5. *(a) EDX spectra of Fe_3O_4-(rGO&CNT) and (b) elemental mapping of Fe_3O_4-(rGO&CNT)*

Voltammetric behavior of imatinib

The cyclic voltammetry (CV) method was used to investigate the electrochemical behaviour of IM on CPE, rGO/CPE, CNT/CPE, rGO&CNT/CPE and Fe_3O_4-(rGO&CNT)/CPE in 0.1 mol L^{-1} PB, pH 7.0. The voltammograms obtained for 50 µmol L^{-1} IM at 100 mV/s are shown in Figure 6(A). According to the results, the oxidation peak current of IM at the surface of the unmodified CPE is ~40 µA, while for rGO/CPE, CNT/CPE, rGO&CNT/CPE and Fe_3O_4-(rGO&CNT)/CPE electrodes, the oxidation peak current values are ~70, ~90, ~110 and ~170 µA, respectively. Moreover, the oxidation potential of IM on the surfaces of CPE and rGO/CPE is ~0.9 V, while the oxidation potential of IM on the surfaces of CNT/CPE, rGO&CNT/CPE and Fe_3O_4-(rGO&CNT)/CPE is ~0.86. Due to the high surface area of the electrode and the effects of rGO, CNT and Fe_3O_4 nanoparticle materials, the oxidation current of Fe_3O_4-(rGO&CNT)/CPE increases. In addition, these points improve the conductivity of Fe_3O_4--(rGO&CNT) composite, which results in a higher oxidation current on the surface of this electrode than on other electrodes.

The 0.1 mol L^{-1} PB with pH 5.0-9.0 was used to detect IM response on the surface of Fe_3O_4--(rGO&CNT)/CPE. As shown in Figure 6 (B), the maximum oxidation current of IM at Fe_3O_4--(rGO&CNT)/CPE was obtained at pH 7.0, then used as the optimal pH for other tests. The dependence of the oxidation peak potential of IM on pH is also shown in Figure 6 (C). The slope of the line obtained for this relation was 54 mV per pH unit, which is close to the slope of the Nernst equation. Accordingly, the number of electrons and protons participating in the oxidation of IM is the same according to Scheme 1.

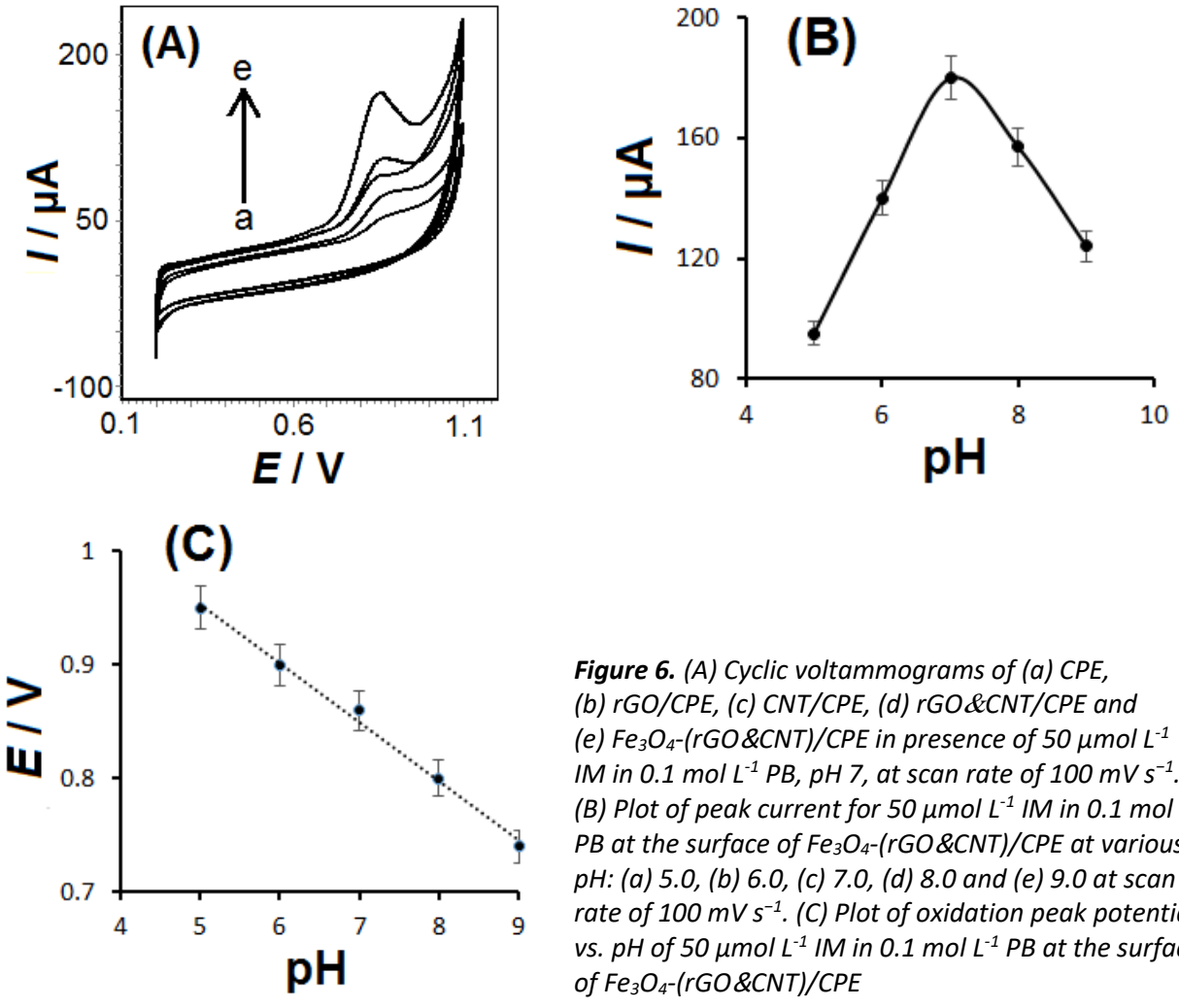

Figure 6. *(A) Cyclic voltammograms of (a) CPE, (b) rGO/CPE, (c) CNT/CPE, (d) rGO&CNT/CPE and (e) Fe_3O_4-(rGO&CNT)/CPE in presence of 50 µmol L^{-1} IM in 0.1 mol L^{-1} PB, pH 7, at scan rate of 100 mV s^{-1}. (B) Plot of peak current for 50 µmol L^{-1} IM in 0.1 mol L^{-1} PB at the surface of Fe_3O_4-(rGO&CNT)/CPE at various pH: (a) 5.0, (b) 6.0, (c) 7.0, (d) 8.0 and (e) 9.0 at scan rate of 100 mV s^{-1}. (C) Plot of oxidation peak potential vs. pH of 50 µmol L^{-1} IM in 0.1 mol L^{-1} PB at the surface of Fe_3O_4-(rGO&CNT)/CPE*

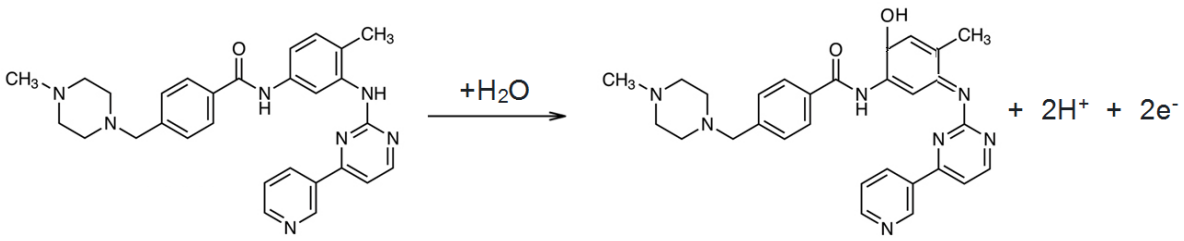

Scheme 1. *Electrochemical oxidation mechanism of IM*

Figure 7 (A) shows the CV curves of Fe_3O_4-(rGO&CNT)/CPE toward IM at different scan rates from 25 to 300 mV s^{-1}. It can be seen that the electrochemical oxidation current (*I*) of IM has a linear relationship with the $v^{1/2}$ (inset) while the oxidation potential is shifted positively with the increase of the scan rate, indicating that the electrochemical reaction of the IM obeyed the diffusion-controlled process. Also, the slope obtained from the graph of log *I* as a function of log *v* is 0.537 (Figure 7B), which is very near to the generally expected slope value of 0.5, showing a purely diffusion-controlled system.

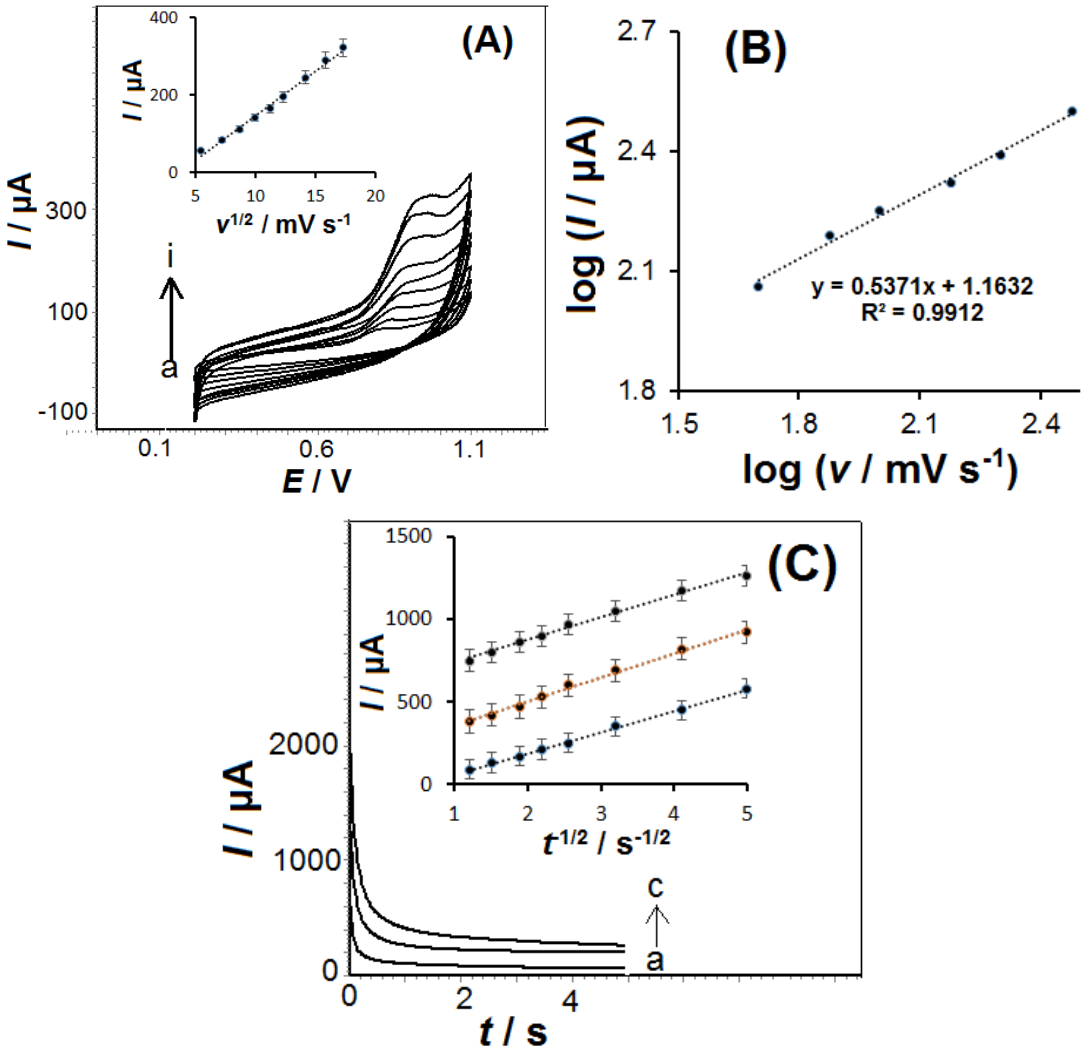

Figure 7. *(A) Cyclic voltammograms of 30 µmol L^{-1} IM in 0.1 mol L^{-1} PB (pH 7.0) and 0.1 mol L^{-1} KCl as supporting electrolyte at the surface of Fe_3O_4-(rGO&CNT)/CPE and various scan rates: (a) 25, (b) 50, (c) 75, (d) 100, (e) 125, (f) 150, (g) 200, (h) 250 and (i) 300 mV s^{-1}; inset: plot of peak currents vs. square root of scan rates. (B) Plot log I as a function of log υ. (C) Chronoamperograms for Fe_3O_4-(rGO&CNT)/CPE in the presence of (a) 50, (b) 100 and (c) 200 µmol L^{-1} IM; (inset) Cottrell's plot for the data from chronoamperograms*

Chromatoamperometry and other electrochemical methods were usually employed to investigate electrode reactions at chemically modified electrodes. Chronoamperometric measurement of IM was done by setting the Fe_3O_4-(rGO&CNT)/CPE working electrode potential at 0.9 V *vs*. Ag/AgCl/$KCl_{(3M)}$ for various concentrations of IM (Figure 7(C)). For IM with a diffusion coefficient of *D*, the current for the electrochemical reaction at a mass transport limited rate is described by the Cottrell equation (2) [32]:

$$I = nFAD^{1/2}c_b\pi^{-1/2}t^{-1/2} \quad (2)$$

where *n*, F, *A*, c_b, *D* and *t* are the number of electrons transferred (2), Faraday constant (96485 C), electrode area (0.27 cm^2), bulk concentration (50, 100 and 200 μmol L^{-1}), diffusion coefficient (cm^2 s^{-1}), and time (s), respectively.

Experimental plots of *I vs*. $t^{-1/2}$ were employed, with the best fits for different concentrations of IM (inset). From the resulting slope and Cottrell equation, the mean value of *D* for IM was calculated as 5.7×10^{-5} cm^2 s^{-1}.

Analytical performance of Fe_3O_4-(rGO&CNT)/CPE sensor

The quantitative analysis of the IM was based on the dependence of the peak current value on the concentration of IM. Cyclic voltammograms depicting the systematic increase in the peak current values with an increase of the concentration in the linear working range 0.1 to 40 μM at Fe_3O_4-(rGO&CNT)/CPE are presented in Figure 8A. The linear calibration plot according to I / μA = 27.22 + + 3.36 c_{IM} / μmol L^{-1} with a correlation coefficient of 0.991 and error bars are presented in the inset. The detection limit (LOD) of 57 nmol L^{-1} was calculated using the formula $3\sigma/\mathbf{b}$, where σ is the standard deviation of the blank and b is the slope of the calibration curve. The calculated value for the limit of quantification (LOQ) is 187.5 nM, while the sensitivity was estimated to be 3.365 μA μM^{-1}.

Table 1 compares the analytical performance of Fe_3O_4-(rGO&CNT)/CPE for IM determination with these obtained by voltammetry techniques at some other electrodes [13,16,33-36]. Based on the results of this study, the Fe_3O_4-(rGO&CNT) modified CPE electrode appears to be comparable to other electrodes in terms of achieving low detection limit, wide range of concentrations (LDR) and high sensitivity. The LOD is, however, higher as compared to other sensors presented in Table 1, but the proposed modified electrode was prepared by a simple, easy, cost-effective and one-step procedure of making Fe_3O_4-(rGO&CNT)/CPE electrode that is more readily available than materials used in preparation of other electrodes. Moreover, there is no proof that a single electrode can work for a long period of time with almost the same performance, which gives the Fe_3O_4--(rGO&CNT)/CPE the privilege of being used for routine work.

The reproducibility of E_p and I_p values was tested by repeating five experiments with 20 μmol L^{-1} of IM. The RSDs were calculated to be 3.43 % for I_p and 1.61 % for E_p, respectively, using CV, which indicates excellent reproducibility. The four consecutive measurements at one electrode in 0.1 mol L^{-1} PB (pH 7.0) containing 20 μmol L^{-1} IM have shown <5 % RSD at optimum pH to investigate Fe_3O_4--(rGO&CNT)/CPE repeatability. Based on this data, it appears that Fe_3O_4-(rGO&CNT)/CPE has appropriate repeatability. Moreover, six measurements were taken during a month to determine the stability of Fe_3O_4-(rGO&CNT)/CPE for IM measurement. In various measurements conducted over one month, the oxidation current changes of IM were 7.83 %, indicating that the electrode is stable.

In order to examine the selectivity of IM, it must be measured concurrently with compounds present in the body or compounds being administered simultaneously with IM. Many minerals in a body contain cations (Na^+, Ca^{2+}, Mg^{+2}, etc.) and anions. For this reason, we investigated possible

interferents for IM detection, such as glucose, cysteine, lysine, Ca^{+2}, K^{+}, Na^{+}, Mg^{+2}, doxorubicin, acetaminophen, and ascorbic acid.

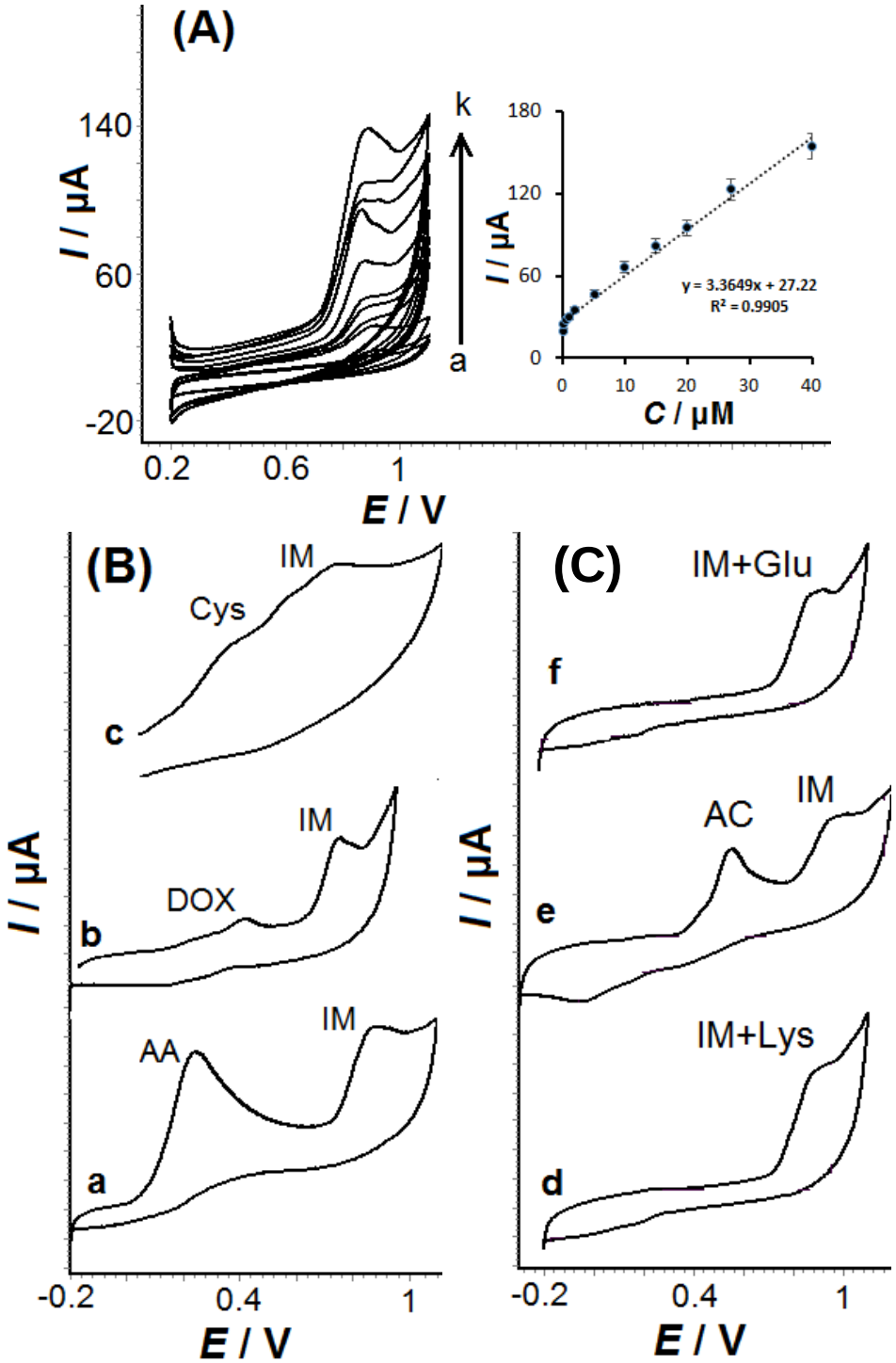

Figure 8. *Cyclic voltammograms of Fe_3O_4-(rGO&CNT)/CPE in 0.1 mol L^{-1} PB (pH 7.0): (A) in the presence of (a) 0.1, (b) 0.2, (c) 0.5, (d) 1, (e) 2, (f) 5, (g) 10, (h) 15, (i) 20, (j) 27 and (k) 40 µmol L^{-1} of IM; Inset: plot of oxidation peak current vs. IM concentration, (B) upon addition of (a) ascorbic acid (AA, 30 µmol L^{-1}) + IM (30 µmol L^{-1}), (b) doxorubicin (DOX, 30 µmol L^{-1}) + IM (30 µmol L^{-1}), (C) cysteine (Cys, 30 µmol L^{-1})+ IM (30 µmol L^{-1}), (d) lysine (Lys, 30 µmol L^{-1}) + IM (30 µmol L^{-1}), (e) acetaminophen (AC, 30 µmol L^{-1}) + IM (30 µmol L^{-1}) and (f) glucose (Glu, 30 µmol L^{-1})+IM (30 µmol L^{-1})*

Some results of IM detection at the Fe_3O_4-(rGO&CNT)/CPE in 0.1M PB (pH 7.0) containing some interferents at equal concentrations as IM, are presented in Figure 8B. As seen in Figure 8B, glucose, cysteine, lysine, doxorubicin, acetaminophen, and ascorbic acid did not cause *any* interference.

Moreover, some results (not shown here) indicated that the 500-fold higher concentrations of glucose and cations (Ca^{+2}, K^+, Na^+ and Mg^{+2}) and 100-fold higher concentrations of lysine, ascorbic acid, acetaminophen and doxorubicin did not affect the determination of IM. However, 5-fold higher concentrations of cysteine showed interference in the determination of IM at Fe_3O_4-(rGO&CNT)/CPE.

Table 1 *Analytical parameters for voltammetric determination of IM at different modified electrodes*

Electrode	Method	Linear range, µmol L^{-1}	LOD, nmol L^{-1}	Sensitivity, µA µmol L^{-1}	Ref.
MWCNT/SPCE	SWV[a]	0.005-0.912	7.0	-	[13]
$TbFeO_3$/g-C_3N_4/GCE	DPV[b]	0.002-100	0.6	5.92 cm^{-2}	[16]
MWCNT/NiO-ZnO/GCE	DPV	0.015-2	2.4	2.64	[33]
Cu-BTC/RGO/GCE	DPV	0.04-80	6.0	-	[34]
RGO/AgNPs/GCE	DPV	0.001-280	1.1	0.17	[35]
Cu-BTC/MWCNT/GCE	DPV	0.01-220	4.1	1.65	[36]
Fe_3O_4-(rGO&CNT)/CPE	CV	0.1-40	57	3.36	this work

[a] Square wave voltammetry
[b] Differential pulse voltammetry

The accuracy of the proposed method was assessed by performing recovery experiments. Human plasma and urine samples were measured using the standard addition method at pH 7.0 on Fe_3O_4-(rGO&CNT)/CPE. Table 2 presents the concentrations of IM added to plasma and urine samples, along with their standard deviations and recovery percentages. According to the results, the mean recovery percentage in real samples is approximately 94-98.5, suggesting that the modified electrode can accurately measure IM. The results obtained from the proposed method were compared with the UV-Vis spectroscopy results (Table 2). It was observed that the results of electrochemical analysis show consistency with those obtained by the UV-Vis method (Figure 9) with acceptable recoveries.

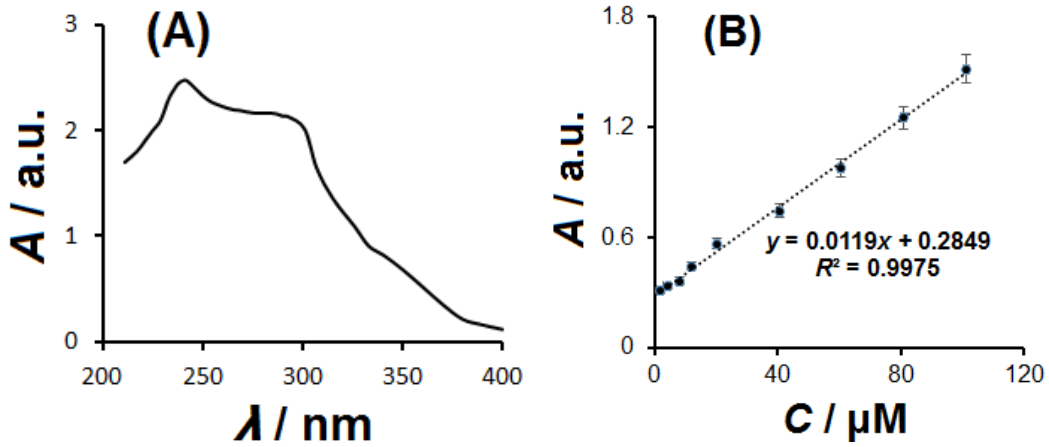

Figure 9. *(A) The UV-Vis spectrum of IM (202.5 µM) in PB solution (pH 7.0); (B) calibration curve of IM determined by UV-Vis spectroscopy*

Table 2. *Determination of IM in urine and blood plasma samples at Fe_3O_4-(rGO&CNT)/CPE in 0.1 mol L^{-1} PB solution (pH 7.0)*

Sample	Amount, µmol L^{-1}		Mean recovery of proposed method, %	Mean recovery of UV-Vis method, %
	Added	Found	(*n*=3)	(*n*=3)
Plasma	10.0	9.5	95.0±4.4	98.0±3.7
Plasma	20.0	19.7	98.5±4.3	102.0±2.9
Urine	10.0	9.4	94.0±2.1	94.0±1.6
Urine	20.0	19.1	95.5±4.1	99.8±3.2

Conclusion

In this study, new rGO sheets have been synthesized *via* a facile and environmentally friendly process using *Callicarpa maingayi* leaf extract. By combining CNT tubes, rGO sheets and Fe_3O_4 nanoparticles, an excellent nanocomposite on the CPE electrode was created with a high surface area and good conductivity, which led to satisfactory results in the IM determination. Due to the increased electron transfer rate at the surface of Fe_3O_4-(rGO&CNT)/CPE electrode at pH 7.0, the oxidation current of IM was higher than at CPE, rGO/CPE, CNT/CPE and rGO&CNT/CPE. The excellent results are attributed to the large electrode surface area provided by CNT, rGO and Fe_3O_4 nanoparticles, as well as their excellent catalytic properties. The proposed Fe_3O_4-(rGO&CNT)/CPE showed fast response, stable measurements, and excellent anti-interference properties. Due to the advantages of magnetism and conductivity, the prepared nanocomposite material could easily adhere to the electrode surface, offering good electrical contact. In addition, Fe_3O_4-(rGO&CNT) nanocomposite-modified CPE can be applied to detect of IM in real samples.

Acknowledgements*: The authors are sincerely thankful for the research facilities provided by the Ayatollah Amoli Branch of the Islamic Azad University.*

References

[1] Y. Liu, M. Wei, Y. Hu, L. Zhu, J. Du, An electrochemical sensor based on a molecularly imprinted polymer for determination of anticancer drug Mitoxantrone, *Sensors and Actuators B* **255** (2018) 544-551. https://doi.org/10.1016/j.snb.2017.08.023

[2] M. Muti, M. Muti, Electrochemical monitoring of the interaction between anticancer drug and DNA in the presence of antioxidant, *Talanta* **178** (2018) 1033-1039. https://doi.org/10.1016/j.talanta.2017.08.089

[3] K. N. Cahill, H. R. Katz, J. Cui, J. Lai, Sh. Kazani, A. Crosby-Thompson, D. Garofalo, M. Castro, N. Jarjour, E. DiMango, S. Erzurum, J. Trevor, K. Shenoy, V. M. Chinchilli, M. E. Wechsler, T. M. Laidlaw, J. A. Boyce, E. Israel, KIT inhibition by imatinib in patients with severe refractory asthma, *The New England Journal of Medicine* **376** (2017) 1911-1920. https://doi.org/10.1056/NEJMoa1613125

[4] P. Sobierajska, A. Serwotka-Suszczak, D. Szymanski, K. Marycz, R. J. Wiglusz, Nanohydroxyapatite-mediated imatinib delivery for specific anticancer applications, *Molecules* **25** (2020) 4602. https://doi.org/10.3390/molecules25204602

[5] A. Hochhaus, R. A. Larson, F. Guilhot, J. P. Radich, S. Branford, T. P. Hughes, M. Baccarani, M. W. Deininger, F. Cervantes, S. Fujihara, Ch. E. Ortmann, H. D. Menssen, H. Kantarjian, S. G. O'Brien, B. J. Druker, Long-term outcomes of imatinib treatment for chronic myeloid leukemia, *The New England Journal of Medicine* **376** (2017) 917-927. https://doi.org/10.1056/NEJMoa1609324

[6] M. A. Babaei, B. Kamalidehghan, M. Saleem, H. Z. Huri, F. Ahmadipour, Receptor tyrosine kinase (c-Kit) inhibitors: a potential therapeutic target in cancer cells, *Drug Design Development Therapy* **10** (2016) 2443-2459. https://doi.org/10.2147/DDDT.S89114

[7] Q. Jiao, L. Bi, Y. Ren, S. Song, Q. Wang, Y. S. Wang, Advances in studies of tyrosine kinase inhibitors and their acquired resistance, *Molecular Cancer* **17** (2018) 36. https://doi.org/10.1186/s12943-018-0801-5

[8] I. Grante, A. Actins, L. Orola, Protonation effects on the UV/Vis absorption spectra of imatinib: A theoretical and experimental study, *Spectrochimica Acta: Molecular and Biomolecular Spectroscopy* **129** (2014) 326-332. https://doi.org/10.1016/j.saa.2014.03.059

[9] O. Roth, O. Spreux-Varoquaux, S. Bouchet, P. Rousselot, S. Castaigne, S. Rigaudeau, V. Raggueneau, P. Therond, P. Devillier, M. Molimard, B. Meneglier, Imatinib assay by HPLC

with photodiode-array UV detection in plasma from patients with chronic myeloid leukemia: Comparison with LC-MS/MS, *Clinica Chimica Acta* **411** (2010) 140-146. https://doi.org/10.1016/j.cca.2009.10.007

[10] G. Bende, S. Kollipara, V. Sekar, R. Saha, UV-spectrophotometric determination of imatinib mesylate and its application in solubility studies, *Pharmazie* **63** (2008) 641-645. https://doi.org/10.1691/ph.2008.8094

[11] J. Rodríguez-Flores, J. B. Nevado, A. C. Salcedo, M. P. Cabello Díaz, Nonaqueous capillary electrophoresis method for the analysis of gleevec and its main metabolite in human urine, *Journal of Chromatography A* **1068** (2005) 175-182. https://doi.org/10.1016/j.chroma.2004.09.089

[12] O. S. Ahmed, M. Malý, Y. Ladner, L. Philibert, P. Dubský, C. Perrin, Influence of salt and acetonitrile on the capillary zone electrophoresis analysis of imatinib in plasma samples, *Electrophoresis* **40** (2019) 2810-2819. https://doi.org/10.1002/elps.201900188

[13] J. Rodríguez, G. Castañeda, I. Lizcano, Electrochemical sensor for leukemia drug imatinib determination in urine by adsorptive striping square wave voltammetry using modified screen-printed electrodes, *Electrochimica Acta* **269** (2018) 668-675. https://doi.org/10.1016/j.electacta.2018.03.051

[14] J. G. Manjunatha, Electroanalysis of estriol hormone using electrochemical sensor, *Sensing and Bio-Sensing Research* **16** (2017) 79-84. https://doi.org/10.1016/j.sbsr.2017.11.006

[15] J. G. Manjunatha, Poly (Nigrosine) Modified Electrochemical Sensor for the Determination of Dopamine and Uric acid: A Cyclic Voltammetric Study, *International Journal of ChemTech Research* **9** (2016) 136-146. https://sphinxsai.com/2016/ch_vol9_no2/1/(136-146)V9N2CT.pdf

[16] M. Baladi, H. Teymourini, E. A. Dawi, M. Amiri, A. Ramazani, M. Salavati-Niasari, Electrochemical determination of imatinib mesylate using TbFeO3/g-C3N4 nanocomposite modified glassy carbon electrode, *Arabian Journal of Chemistry* **16** (2023) 104963. https://doi.org/10.1016/j.arabjc.2023.104963

[17] J. G. Manjunatha, Electrochemical polymerised graphene paste electrode and application to catechol sensing, *The Open Chemical Engineering Journal* **13** (2019) 81-87. https://doi.org/10.2174/1874123101913010081

[18] G. Tigari, J. G. Manjunatha, Optimized voltammetric experiment for the determination of phloroglucinol at surfactant modified carbon nanotube paste electrode, *Instruments and Experimental Techniques* **63** (2020) 750-757. https://doi.org/10.1134/S0020441220050139

[19] A. U. Alam, D. Clyne, H. Jin, N. X. Hu, M. J. Deen, *ACS Sensors* **5** (2020) 412-422. https://doi.org/10.1021/acssensors.9b02095

[20] S. Morais, Advances and applications of carbon nanotubes, *Nanomaterials* **13** (2023) 2674. https://doi.org/10.3390/nano13192674

[21] A. Hosseini Fakhrabad, R. Sanavi Khoshnood, M. R. Abedib, M. Ebrahimi, Fabrication a composite carbon paste electrodes (CPEs) modified with multi-wall carbon nanotubes (MWCNTs/N, N-Bis (salicyliden)-1,3- propandiamine) for determination of lanthanum (III), *Eurasian Chemical Communications* **3** (2021) 627-634. https://www.echemcom.com/article_134775_efa87e18e1e4daddba676005d78a6feb.pdf

[22] A. B. Monnappa, J. G. Manjunatha, A. Sripathi Bhatt, H. Nagarajappa, Sensitive and selective electrochemical detection of vanillin at graphene based poly (methyl orange) modified electrode, *Journal of Science: Advanced Materials and Devices* **6** (2021) 415-424. https://doi.org/10.1016/j.jsamd.2021.05.002

[23] Ch. Zou, J. Hu, Y. Su, F. Shao, Z. Tao, T. Huo, Zh. Zhou, N. Hu, Zh. Yang, E. Siu-Wai Kong, Y. Zhang, Three-dimensional Fe_3O_4@reduced graphene oxide heterojunctions for high-performance room-temperature NO_2 sensors, *Frontiers in Materials* **6** (2019) 195. https://doi.org/10.3389/fmats.2019.00195

[24] G. J. Rani, K. J. Babu, M. J. Rajan, Watsonia meriana flower like Fe_3O_4/reduced graphene oxide nanocomposite for the highly sensitive and selective electrochemical sensing of dopamine, *Journal of Alloys and Compounds* **688** (2016) 500-512. https://doi.org/10.1016/j.jallcom.2016.07.101
[25] E. Aliyev, V. Filiz, M. M. Khan, Y. J. Lee, C. Abetz, V. Abetz, Structural characterization of graphene oxide: surface functional groups and fractionated oxidative debris, *Nanomaterials* **9** (2019) 1180. https://doi.org/10.3390/nano9081180
[26] E. Vatandost, A, Ghorbani-HasanSaraei, F. Chekin, Sh. Naghizadeh Raeisi, S. A. Shahidi, Green tea extract assisted green synthesis of reduced graphene oxide: Application for highly sensitive electrochemical detection of sunset yellow in food products, *Food Chemistry X* **6** (2020) 100085-100090. https://doi.org/10.1016/j.fochx.2020.100085
[27] N. Hazhir, F. Chekin, J. B. Raoof, Sh. Fathi, A porous reduced graphene oxide/chitosan-based nanocarrier as a delivery system of doxorubicin, *RSC Advances* **9** (2019) 30729-30735. https://doi.org/10.1039/C9RA04977K
[28] A. Negi, K. Dobhal, P. Ghildiyal, Antioxidant potential and effect of extraction solvent on total Phenol content, flavonoids, *International Journal of Pharmaceutical Sciences Review and Research* **49** (2018) 19-24. https://doi.org/10.13140/RG.2.2.14158.15687
[29] Sh. Nikkhah, H. Tahermansouri, F. Chekin, Synthesis, characterization, and electrochemical properties of the modified graphene oxide with 4,4'-methylenedianiline, *Materials Letters* **211** (2018) 323-327. https://doi.org/10.1016/j.matlet.2017.10.037
[30] B. Zareyy, F. Chekin, Sh. Fathi, NiO/porous reduced graphene oxide as active hybrid electrocatalyst for oxygen evolution reaction, *Russian Journal of Electrochemistry* **55** (2019) 333-338. https://doi.org/10.1134/S102319351903011X
[31] L. Shen, J. Dong, B. Wen, X. Wen, J. Li, Facile synthesis of hollow Fe_3O_4-rGO nanocomposites for the electrochemical detection of acetaminophen, *Nanomaterials* **13** (2023) 707. https://doi.org/10.3390/nano13040707
[32] B. Davarnia, S. A. Shahidi, H. Karimi-Maleh, A. Ghorbani HasanSaraei, F. Karimi, Biosynthesis of Ag nanoparticle by peganum harmala extract; antimicrobial activity and ability for fabrication of quercetin food electrochemical sensor, *International Journal of Electrochemical Science* **15** (2020) 2549-2560. https://doi.org/10.20964/2020.03.70
[33] H. Chen, K. Luo, K. Li, A facile electrochemical sensor based on NiO-ZnO/MWCNT-COOH modified GCE for simultaneous quantification of imatinib and itraconazole, *Journal of The Electrochemical Society* **166** (2019) B697-B707. https://doi.org/10.1149/2.1071908jes
[34] N. Rezvani Jalal, T. Madrakian, A. Afkhami, A. Ghoorchian, In situ growth of metal–organic framework HKUST-1 on graphene oxide nanoribbons with high electrochemical sensing Performance in imatinib determination, *ACS Applied Materials & Interfaces* **12** (2020) 4859-4869. https://doi.org/10.1021/acsami.9b18097
[35] Z. Wu, J. Liu, M. Liang, H. Zheng, Ch. Zhu, Y. Wang, Detection of imatinib based on electrochemical sensor constructed using biosynthesized graphene-silver nanocomposite, *Frontiers in Chemistry* **9** (2021) 670074. https://doi.org/10.3389/fchem.2021.670074
[36] B. H. Pour, N. Haghnazari, F. Keshavarzi, E. Ahmadi, B. R. Zarif, High sensitive electrochemical sensor for imatinib based on metal-organic frameworks and multiwall carbon nanotubes nanocomposite, *Microchemical Journal* **165** (2021) 106147. https://doi.org/10.1016/j.microc.2021.106147